ELSEVIER

Catalysis Today 46 (1998) 37–54

CATALYSIS TODAY

Deactivation of bi- and multimetallic reforming catalysts: influence of alloy formation on catalyst activity

N. Macleod*, J.R. Fryer, D. Stirling, G. Webb

Department of Chemistry, University of Glasgow, Glasgow, G12 8QQ, UK

Abstract

A number of bi- and multimetallic reforming catalysts including Pt–Re, Pt–Ir, Pt–Sn, Pt–Ge and Pt–Ir–Ge were prepared and studied in this work. The alloy particles formed in these systems were analysed using transmission electron microscopy (TEM) and energy dispersive X-ray analysis (EDX). *n*-Octane reforming experiments were also performed using a pressurised microreactor system. Tin and germanium were found to modify the properties of these catalysts mainly via a geometric effect. However, formation of bulk Pt–Sn and Pt–Ge alloys contributed to the overall rate of deactivation of these systems. In the case of Pt–Ir and Pt–Re, metallic rhenium and iridium provided sites for the hydrogenolysis of coke deposits resulting in improved resistance to deactivation.

Keywords: Bimetallic; Reforming; *n*-Octane; TEM; EDX; Iridium

1. Introduction

The first bimetallic naphtha reforming catalyst, Pt–Re/Al_2O_3 [1], was introduced in the late 1960s and offered improved activity and stability compared to its monometallic Pt/Al_2O_3 predecessor. A number of bimetallic systems have since been introduced including Pt–Ir [2], Pt–Sn [3] and Pt–Ge [4], all of which have improved properties. Although these bimetallic catalysts have been in use for many years, there is still considerable debate about how the second metal brings about the observed improvement in catalytic properties.

In the case of Pt–Re, Pt–Sn and Pt–Ge the oxidation state of the second metal is still unclear, as is whether or not alloy formation with platinum occurs. From the available literature on these systems it is clear that the observed state of the added metal is highly dependent on a number of factors including the starting materials employed, the metal loadings, the calcination and reduction temperatures and the support used.

Depending on these factors, these three promoters may be found: (a) in the reduced form alloyed with platinum, (b) in an oxidised form stabilised by the support, or (c) as a combination of both of the above, e.g. Re [5–11], Sn [12–19], Ge [20–25]. In the case of Pt–Ir catalysts the situation is somewhat clearer in that iridium is more readily reduced than platinum and is therefore always present as iridium metal [26–33]. Due to the high hydrogenolysis activity of metallic iridium [32], and also rhenium, catalysts containing these metals are treated with sulphur prior to use in order to passivate this high activity. When the added

*Corresponding author. Present address: Department of Chemistry, University of Cambridge, Cambridge, CB2 1EW, UK.
E-mail: nm235@cam.ac.uk

0920-5861/98/$ – see front matter
PII: S0920-5861(98)00349-6

metal is inactive, such as Sn or Ge, no such treatment is required.

The main theories put forward to account for the improved properties of bimetallic catalysts tend to involve either geometric and/or electronic effects. Electronic modification of platinum particles may be induced by an interaction with an oxide layer of the promoter [15] or by alloy formation [34]. This results in a weakening of the Pt–C bond strength on adsorption of alkane reactants and hence alters the activity and selectivity of the catalysts. This type of interaction is also thought to make the catalyst less susceptible to deactivation by the deposition of carbonaceous species onto the metal surface [12,35,36].

Geometric (ensemble) effects arise due to the different structure sensitivities of the reactions that occur in reforming. Undesirable processes such as hydrogenolysis and coke formation are known to require relatively large clusters or ensembles of adjacent metal atoms whilst desirable reactions such as aromatisation and isomerisation can occur on single isolated atoms [35,37]. Therefore diluting the active platinum surface into smaller ensembles by the addition of an inactive species such as Sn or Ge selectively poisons hydrogenolysis and improves the catalysts' resistance to deactivation. In the case of sulphided Pt–Re, sulphur binds preferentially to Re due to the greater bond strength between Re–S as compared with Pt–S. For this reason Re–S is often considered to be an inert dilutant which modifies the catalyst in a similar manner to Sn [38]. Indeed a number of studies have concluded that addition of rhenium to these catalysts is only beneficial to the overall reforming properties if the catalyst is also treated with sulphur [36,38].

Other studies, however, have concluded that the presence of metallic rhenium or iridium atoms on the metal surface improves the properties of these catalysts by supplying sites for the hydrogenation/hydrogenolysis of coke deposits or the precursors of coke [39,40], thereby reducing deactivation. A number of studies have also found that Pt–Ir alloy particles are considerably more active than either Pt or Pt–Re particles [33,40].

The presence of oxidised promoter species may also influence the catalytic properties of these systems in a number of ways not directly involving platinum. It has been found that the presence of Sn(II) species poisons the highly acidic sites on alumina thereby reducing the hydrocracking activity [15]. Conversely, in the case of Pt–Ge, the presence of acidic GeO_2 increased the hydrocracking activity of these catalysts [25,41].

Previous studies in this laboratory [42–45], employing transmission electron microscopy and energy dispersive X-ray analysis, investigated alloy formation in Pt–Re, Pt–Sn and Pt–Ge/γ-Al_2O_3 catalysts. It was found that after calcination and reduction at 400°C the second metal in each of these three systems was present mainly as a highly dispersed oxide. In the case of Pt–Sn and Pt–Ge, however, after use in the reforming of *n*-octane at 510°C for a number of hours, it was found that reduction of the second metal and alloy formation had occurred. A number of alloy phases were identified in both systems [43–45]. In the case of Pt–Re, no alloy particles were detected after reforming and it was concluded that the rhenium component remained as a highly dispersed oxide phase [42].

The aim of the present study is to extend this work to include iridium containing catalysts and to investigate the influence of alloy formation on the corresponding catalytic properties in a number of these systems. It was also hoped that the high hydrogenolysis activity of iridium would provide a useful probe to investigate geometric effects in these catalysts.

2. Experimental

2.1. Catalyst preparation

The following catalysts were prepared and tested:

1. 0.3 wt% Pt/Al_2O_3,
2. 0.3 wt% Pt–0.3 wt% Sn/Al_2O_3,
3. 0.3 wt% Pt–0.3 wt% Ge/Al_2O_3,
4. 0.3 wt% Pt–0.3 wt% Re/Al_2O_3 (EuroPt 4),
5. 0.3 wt% Pt–0.3 wt% Ir/Al_2O_3,
6. 0.3 wt% Pt–0.3 wt% Ir–0.03 wt% Ge/Al_2O_3,
7. 0.3 wt% Pt–0.3 wt% Ir–0.3 wt% Ge/Al_2O_3,
8. 0.3 wt% Ir/Al_2O_3,
9. 0.3 wt% Ir–0.3 wt% Ge/Al_2O_3, and
10. 0.3 wt% Ir–0.55 wt% V_2O_5/Al_2O_3.

These catalysts will be referred to in the remainder of the text by simply stating the metals that they contained, e.g. catalyst 2 will be referred to as

Pt–Sn. Catalysts 6 and 7 will be distinguished by referring to them as Pt–Ir–0.03Ge and Pt–Ir–0.3Ge, respectively.

Each catalyst, with the exception of Pt–Re, was prepared during the course of this study using a standard wet impregnation technique. The support used in each case was a commercial pelletised γ-Al_2O_3 (CK300, BET area 200 m^2/g) consisting of cylindrical pellets about 2 mm in diameter and ranging from 2 to 10 mm in length. The catalysts were prepared by a coimpregnation route employing dilute HCl solutions of the appropriate metal salts, i.e., H_2PtCl_6, $SnCl_2{\cdot}2H_2O$ and $IrCl_3{\cdot}3H_2O$. In the case of germanium, a hydrochloric acid solution of Ge(IV) was used (germanium ICP/DCP standard solution, Aldrich, 10 200 μg/ml). After impregnation, the catalyst precursors were dried at 110°C for 4 h in air. This was followed by the following activation procedures:

1. *Calcination*. Heated from room temperature to 400°C at 5°C/min in flowing air (60 ml/min) then held at this temperature for 4 h, followed by cooling to room temperature in flowing air.
2. *Flushing*. He (60 ml/min) was passed over the catalyst for 1 h at room temperature.
3. *Reduction*. The reduction was carried out in flowing H_2 (60 ml/min), with a programmed temperature increase of 5°C/min from room temperature to 400°C and maintained at this temperature for 2 h. The catalyst was then cooled to room temperature in flowing hydrogen.

Finally, passivation was carried out in a 1% air/He mix.

2.2. Electron microscopy and EDX

The microscope used was a TOPCON-EM002B instrument in which the EDX system LINK 200-QX was installed. The microscope was operated at 200 kV with a LaB_6 filament. The point to point resolution of the instrument was 1.8 Å. The energy resolution of the EDX system was 138 eV at 5.9 keV.

TEM specimens were prepared by placing a drop of ethanol solution, containing the ground catalyst powder in suspension, onto a carbon-film coated copper grid.

The combination of microbeam electron diffraction (MBED) and energy dispersive X-ray analysis (EDX) was used to identify the alloy phases present in these catalysts. MBED patterns and EDX spectra were obtained from individual particles by focusing the electron beam onto the particle under examination. The minimum beam diameter obtainable was 2 nm. The collection time for EDX spectra was usually 100 s. During collection the beam was sometimes momentarily spread (under or over focused) to obtain an image of the particle and then relocated to compensate for any specimen drift. The sensitivity of the EDX system was about 400–800 platinum atoms, or between 2 and 3 nm particle size.

A double tilt ($\pm 10^\circ$) specimen stage was used to obtain zone-axis microbeam diffraction patterns for particles. Beam tilt was sometimes used for final precise crystal alignment to obtain zone-axis MBEDs. The MBED pattern for platinum, the elemental identity of which was verified by EDX, was used as an in situ standard for the calibration of the camera length. All the MBEDs were recorded at the same camera length of 11 cm and are printed in the text at the same optical enlargement.

The procedure for performing quantitative EDX analysis in the Pt–Sn and Pt–Ge systems has been described previously [43,44]. In the case of the Pt–Ir system, due to the proximity of these metals in the periodic table, there is considerable overlap of X-ray intensity. The M lines (Pt M – 2.05 keV, Ir M – 1.98 keV) were completely unresolved and there was also considerable overlap of the L_{α_1} lines (Pt L_{α_1}– 9.441 keV, Ir L_{α_1} – 9.173 keV). The Ir L_{α_1} was also somewhat obscured due to its proximity to the large Cu K_β systems peak (8.907 keV). Approximate quantitative analysis was performed using the L_{β_1} peaks (Pt L_{β_1} – 11.069 keV, Ir L_{β_1} – 10.706 keV) although the low intensities of these lines and a certain degree of overlap reduced the accuracy of the results obtained. The k factors for these two metals were sufficiently near one another to allow atomic ratios to be estimated directly from intensity data.

For trimetallic alloys containing Pt, Ir and Ge the Pt L_{β_1} and Ir L_{β_1} lines were first used to obtain a value of Pt/Ir. The concentration of Ge was then related to this value using the sum of the Pt M and Ir M lines and the Ge K_α line. Using the relevant k factors the following relationship for atomic ratios was obtained:

$$\frac{\mathrm{Pt}+\mathrm{Ir}}{\mathrm{Ge}} = 0.35\frac{I_{\mathrm{Pt}_M}+I_{\mathrm{Ir}_M}}{I_{\mathrm{Ge}}K_\alpha},$$

where I=intensity of X-ray line.

2.3. Catalyst testing

n-Octane reforming was carried out in a microreactor which will be described elsewhere [46]. The reaction conditions used were as follows: H_2/*n*-octane=6/1; temperature=510°C; pressure=860 kPa; weight hourly space velocity=2 h^{-1}. Analysis of the reaction products was carried out by sampling to a Shimadzu gas chromatograph.

The yield, conversion and selectivity values quoted in this work are defined as follows:

$$\text{yield } (\%) = \frac{n_i(M_i)}{N(X)} \times \frac{100}{1},$$

$$\text{conversion } (\%) = \frac{\sum_{i=1}^{i=j} n_i(M_i)}{N(X)} \times \frac{100}{1},$$

$$\text{selectivity } (\%) = \frac{n_i(M_i)}{\sum_{i=1}^{i=j} n_i(M_i)} \times \frac{100}{1},$$

where n_i is the number of carbon atoms in product species i, M_i the number of moles of product species i, N the number of carbon atoms in the reactant molecule, X the number of moles of hydrocarbon reactant, and j is the total number of product species.

The total selectivity to aromatic products is defined as the sum of the selectivities to the individual aromatic products. Similarly the selectivity to isomerisation is defined as the sum of the selectivities to i-octane and i-heptane. For hydrocracking the total selectivity values quoted refer only to the desirable hydrocracked products, i.e., i-butane, i-pentane and i-hexane. The selectivity to hydrogenolysis is defined simply as the selectivity to methane.

2.4. Carbon monoxide and oxygen chemisorption

The chemisorption studies were performed as detailed previously [42,43,47]. To extend the work on Pt–Re [42], Pt–Sn [43] and Pt–Ge [45], three iridium containing catalysts were studied, namely: Ir, Ir–Ge and Pt–Ir–0.3Ge. Each catalyst was reduced at 400°C in flowing hydrogen for 2 h prior to the adsorption experiments.

3. Results

3.1. TEM and EDX

3.1.1. Catalysts after calcination and reduction

All the Pt, Pt–Ge, Pt–Sn and Pt–Re/Al_2O_3 catalysts showed similar features after calcination and reduction. Only a small number of particles larger than 1–2 nm were observed in each case and EDX analysis revealed that these were all platinum. Fig. 1 gives an example from the calcined, reduced Pt–Ge/Al_2O_3 catalyst. This [0 1 1] oriented particle was 4 nm in diameter and the 0.227 nm {1 1 1} and 0.196 nm {0 0 2} platinum lattice fringes are visible. The EDX spectrum obtained (inset) confirmed that it was platinum. The Cu signal in this spectrum originated from the copper TEM support grids used and the Al and O peaks from the alumina support.

As was reported previously [43,45], these TEM observations, in conjunction with chemisorption studies, suggest that the Ge, Sn and Re in these catalysts was present mainly as highly dispersed oxide phase after these treatments. The possibility that a few per cent of these metals was reduced and alloyed with platinum could not be ruled out, however.

The Pt–Ir, Pt–Ir–0.03Ge and Pt–Ir–0.3Ge catalysts also showed similar features to one another after calcination and reduction. In this case, however, the majority of metal particles detected were platinum–iridium alloys. Fig. 2 shows a particle from the Pt–Ir catalyst. The lattice fringes visible had a spacing approximately equal to Pt {1 1 1}. The EDX spectrum obtained from this particle (inset) clearly showed the presence of Pt and Ir with an atomic ratio of Pt/Ir≈1.5. This particle was a solid solution. The MBED pattern obtained (inset) was indexed as the [1 2 1] pattern of crystalline platinum. Any variation in lattice parameter due to alloying was too small to be detected (both Pt and Ir are fcc and their lattice parameters differ by only ≈2%). Also imaged in this micrograph were a number of sub 1 nm particles (arrowed). It must be remembered that the majority of the metal particles observed in these catalysts were of this size and therefore too small to be analysed. The dark circular area surrounding the larger particle was caused by contamination by carbon during EDX analysis.

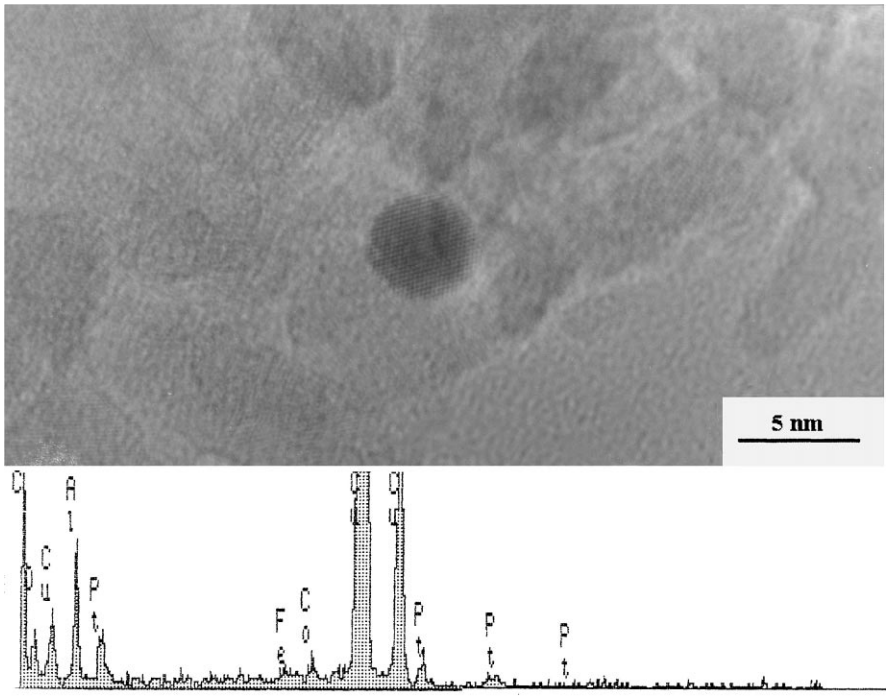

Fig. 1. Pt–Ge catalyst after calcination and reduction. TEM micrograph and corresponding EDX spectrum.

The composition of individual Pt–Ir alloy particles detected in these catalysts was seen to vary about the nominal 1:1, with some Pt-rich and Ir-rich particles observed in each catalyst.

In the Pt–Ir–0.03Ge and Pt–Ir–0.3Ge catalysts, no germanium alloys or germanium particles were detected at this stage, again suggesting that germanium was present as a highly dispersed oxide. Fig. 3 shows a micrograph from the Pt–Ir–0.3Ge catalyst. This particle was about 10 nm in diameter and the EDX spectrum obtained (inset) gave a Pt/Ir ratio of 1.3. The inserted MBED pattern was indexed as the [0 1 1] pattern of crystalline platinum.

3.1.2. Pt–Ge and Pt–Sn after use in reforming

Samples of these catalysts were analysed by TEM after various lengths of time on line (up to 140 h). This was done in order to monitor the formation of alloy particles over time in these systems.

For Pt–Sn, where after calcination and reduction all the detectable metal particles were platinum, after 4 h on line in the reforming of *n*-octane at 510°C the majority of detectable particles were alloys. An example is shown in Fig. 4. This particle was approximately 9 nm in diameter and the inserted EDX spectrum gave a Pt/Sn ratio of 1.0. Some sintering of the metal component was seen to have occurred during this 4 h period.

Similar observations were made with the Pt–Ge catalysts after 4 h on line, as shown in Fig. 5. This particle was approximately 10 nm in diameter and was observed to contain two separate regions. The EDX spectrum obtained from the whole particle gave a Pt/Ge ratio of 3.2. The lattice spacing in both sections of this particle could be indexed to platinum, although to different lattice planes. The lattice near the top of the page was indexed as Pt {1 1 1} with a spacing of 0.227 nm while the lower lattice had a spacing of 0.196 nm corresponding to Pt {0 0 2}. However, it is observed that every second dark band in the lower lattice is much more intense than those between. This is characteristic of a modified or superlattice structure which is known to occur due to alloy formation between platinum and germanium [44].

With longer periods of time on line for both Pt–Ge and Pt–Sn, further sintering of the metal component

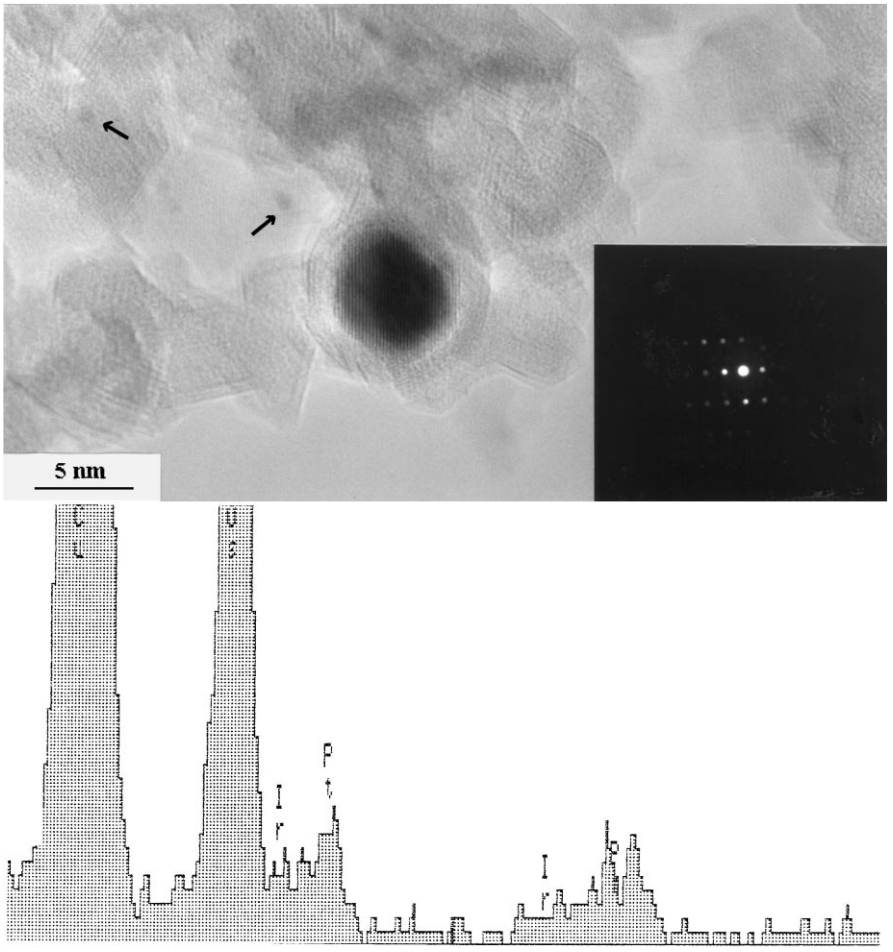

Fig. 2. Pt–Ir catalysts after calcination and reduction. TEM micrograph and corresponding EDX spectrum. Pt/Ir atomic ratio=1.5. Insert: MBED pattern index as [1 2 1] pattern of platinum.

was observed. A number of different alloy phases were formed in each system as previously reported [43–45]. In addition to those alloys previously reported for Pt–Sn, a superlattice Pt–Sn phase was also observed. An example of this phase is shown in Fig. 6. Again this particle was seen to contain two different regions. An EDX spectrum obtained from the smaller left hand region (spectrum A) gave a Pt/Sn ratio of 0.8 and this was assigned to the hcp PtSn structure. The EDX spectrum from the larger right hand area (spectrum B) gave a Pt/Sn ratio of 3.0. An MBED pattern obtained from this area (insert) could be indexed to the Pt [0 1 1] pattern (bright spots) with an extra set of (weaker) spots between. Again this is characteristic of a superlattice structure similar to that already reported for Pt–Ge [45].

3.1.3. *Pt–Re after use in reforming*

No Pt–Re alloy particles were detected in this catalyst even after 140 h on line. The only metallic particles detected were platinum, as shown in Fig. 7. Although no Pt–Re alloys were detected, some sintering of the metal was observed to have occurred. The particle shown in Fig. 7 was approximately 10 nm in diameter and the inserted MBED pattern was indexed as the [1 1 0] crystalline Pt pattern. The corresponding EDX spectrum did not show any evidence for the presence of rhenium. However, it cannot be ruled out

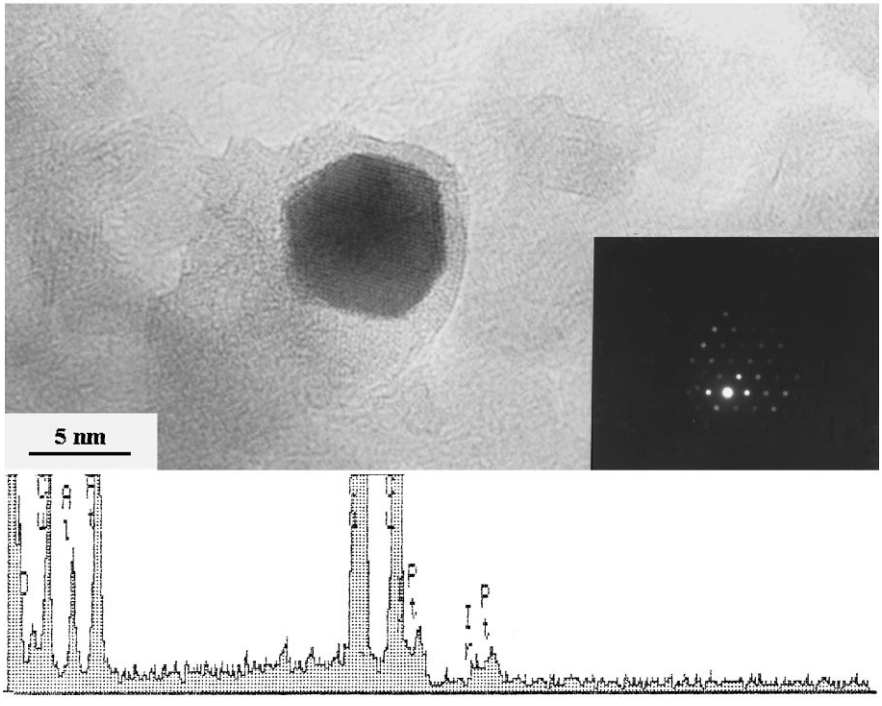

Fig. 3. Pt–Ir–0.3Ge catalyst after calcination and reduction. TEM micrograph and corresponding EDX spectrum. Pt/Ir atomic ratio=1.3. Insert: MBED pattern indexed as [0 1 1] pattern of platinum.

that a small percentage of rhenium was present in this and similar particles.

3.1.4. *Pt–Ir and Pt–Ir–0.03Ge after use in reforming*

In both these catalysts some sintering of the Pt–Ir component was observed. However, for the Pt–Ir–0.03Ge catalyst no germanium alloys were detected. An example is shown in Fig. 8. This particle was approximately 11 nm in diameter. The EDX spectrum gave a Pt/Ir ratio of 1.2 and the corresponding MBED pattern was again indexed as the [0 1 1] pattern of platinum. It is likely that some of the germanium present in this catalyst was present in the reduced form, as with the Pt–Ge catalyst, although the concentration of Ge^0 in the vicinity of any one particle was insufficient to allow detection by the EDX system.

3.1.5. *Pt–Ir–0.3Ge after use in reforming*

In this catalyst the concentration of germanium was sufficient to allow the formation of bulk germanium alloys. An example is given in Fig. 9. This was a relatively large sintered particle although smaller alloys were also observed.

EDX analysis of two regions of this particle (marked A and B) performed with a 5 nm diameter electron probe revealed that the composition of the particle was not uniform. Region A (spectrum A) was found to be rich in iridium and germanium, Pt/Ir=0.8, Pt+Ir/Ge=1.3, whilst region B (spectrum B) was found to be mainly platinum with only a small fraction of iridium. The concentration of germanium was also much lower, Pt+Ir/Ge=4.2. The inserted MBED pattern, taken from region B, contained superlattice reflections (similar to Fig. 6). The bright spots correspond to Pt [0 1 1] whilst the darker spots between the bright spots correspond to the superlattice reflections. The bold lattice fringes visible in region B had a spacing of 0.45 nm, twice the Pt {1 1 1} spacing. Again this is characteristic of the superlattice structure.

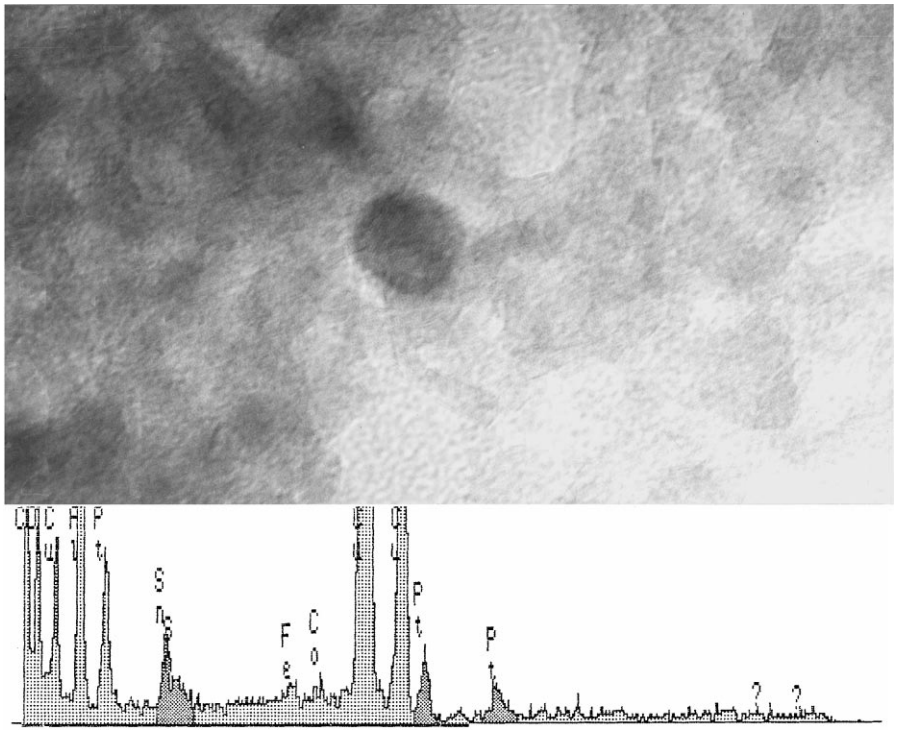

Fig. 4. Pt–Sn catalyst after 4 h on line. TEM micrograph and corresponding EDX spectrum from particle. Pt/Sn atomic ratio=0.9.

3.1.6. *Ir, Ir–Ge and Ir–V catalysts*

No metal particles large enough to be analysed were detected in these systems even after 140 h on line. Fig. 10 shows a typical region of the support for the Ir–Ge catalysts after use in reforming. It is clear that iridium is much more resistant to sintering than platinum in the hydrogen-rich atmospheres used in these studies. One possible explanation for this finding is that iridium has a higher melting point than platinum (Ir – 2443°C, Pt – 1769°C).

3.2. *n-Octane reforming*

3.2.1. *Pt, Pt–Sn, Pt–Ge, Pt–Re and Pt–Ir*

A graph of conversion versus time on line for these catalysts is given in Fig. 11. It is clear that the Pt/Al_2O_3 catalyst showed the fastest initial deactivation. This initial rapid deactivation of platinum catalysts is well documented and is due mainly to coke formation on the metal surface [41]. The Pt–Sn and Pt–Ge catalysts were initially more resistant to deactivation. However, with increasing time on line the rate of deactivation of these catalysts increased. Indeed, for the Pt–Sn catalyst, after approximately 120 h on line the conversion of *n*-octane on this catalyst dropped below the value for the monometallic platinum catalyst. Given a sufficiently long period of time it is likely that the conversion over the Pt–Ge would also fall below platinum.

The rate of deactivation over Pt–Re and Pt–Ir remained low throughout the entire length of the reforming run.

The selectivities to the four major reforming reactions for these catalysts are given in Table 1. The initial values quoted were those obtained after 1 h on line and the final values those after 140 h on line.

The low initial values for aromatisation, isomerisation and hydrocracking over the Pt–Ir catalysts were due to the very high hydrogenolysis activity of this catalyst. It must be remembered that industrial Pt–Ir and Pt–Re catalysts are treated with sulphur before use to decrease this activity.

The selectivity to aromatics over Pt, Pt–Sn and Pt–Ge followed a similar pattern to conversion over these

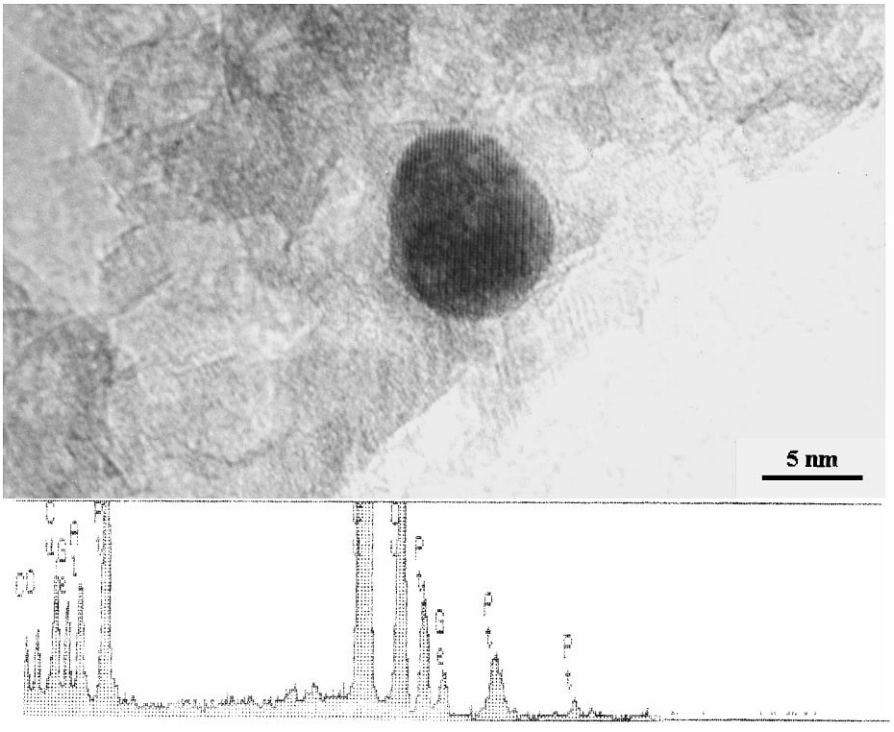

Fig. 5. Pt–Ge catalyst after 4 h on line. TEM micrograph and corresponding EDX spectrum from particle. Pt/Ge atomic ratio=2.8.

catalysts. The selectivity over Pt decreased rapidly initially followed by a period of more gradual decline. The rate of loss of selectivity to aromatics over Pt–Sn and Pt–Ge remained at a more constant level throughout the run. The overall result was that, although Pt–Sn and Pt–Ge were initially more selective than Pt, by 140 h on line the selectivities to aromatics over these three catalysts were similar. It seems that the use of Pt–Sn and Pt–Ge catalysts offers improvements in selectivity to aromatics only for an initial period. With extended use it is likely that the selectivity of Pt–Sn and Pt–Ge would actually drop below that of monometallic platinum.

For Pt–Re it was found that the selectivity to aromatics was stable throughout the run with only a small decrease having occurred. For Pt–Ir the selec-

Table 1
Selectivities to the major reforming reactions over Pt, Pt–Sn, Pt–Ge, Pt–Re and Pt–Ir catalysts (initial values (*I*) obtained after 1 h on line, final values (*F*) obtained after 140 h on line)

Reaction	Selectivity									
	Pt		Pt–Sn		Pt–Ge		Pt–Re		Pt–Ir	
	I	*F*	*I*	*F*	*I*	*F*	*I*	*F*	*I*	*F*
Aromatisation	45.2	25.1	51.0	25.8	43.9	26.2	46.1	44.7	21.7	35.8
Isomerisation	6.5	26.9	2.4	21.0	4.5	25.3	1.1	7.1	0.0	0.0
Hydrocracking	17.1	15.2	15.9	16.3	17.7	18.3	14.9	16.9	1.4	7.5
Hydrogenolysis	6.8	4.6	6.1	5.1	5.3	4.1	10.0	5.2	42.8	22.3

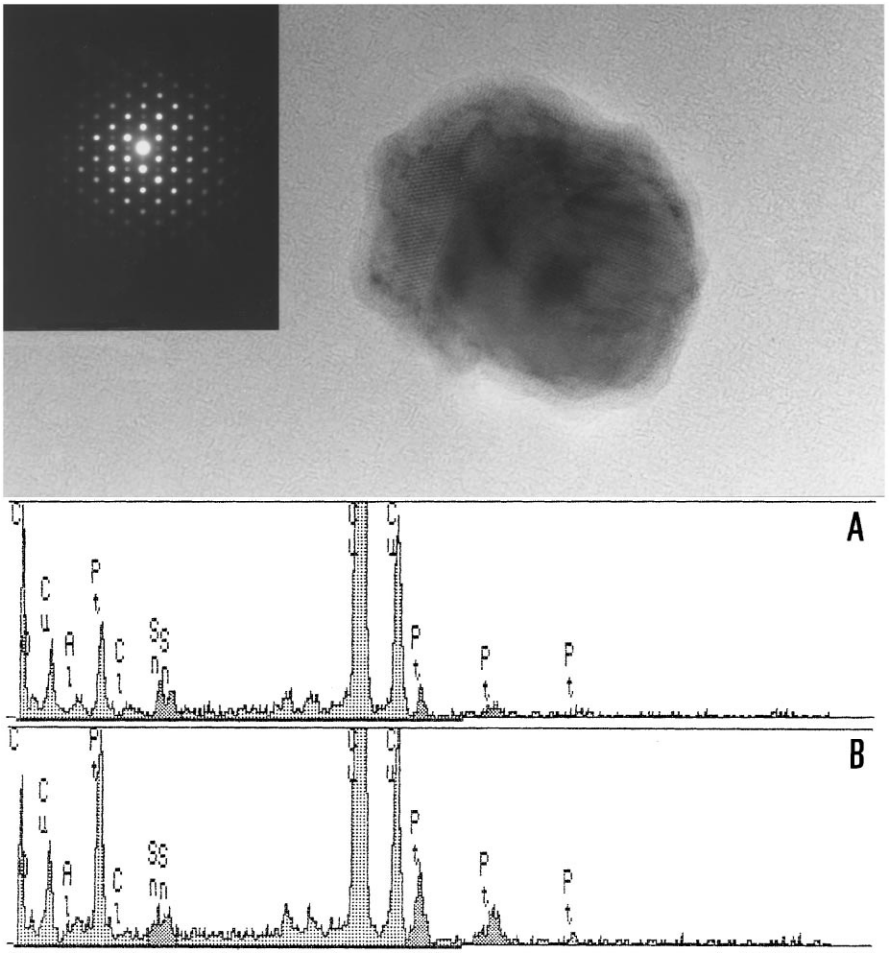

Fig. 6. Pt–Sn catalysts after 140 h on line. TEM micrograph and corresponding EDX spectra. Region A (a) – Pt/Sn atomic ratio=0.8. Region B (b) – Pt/Sn atomic ratio=3.0. Insert: MBED pattern from region B indexed as platinum [0 1 1] (bright spots) with extra supperlatice reflections.

tivity to aromatics increased continuously as the high hydrogenolysis activity of this catalyst was gradually poisoned by coke formation on the metal.

As the selectivity to aromatics over Pt, Pt–Sn and Pt–Ge gradually decreased, a corresponding increase in selectivity to isomerisation was seen to occur. The hydrocracking selectivities remained relatively constant, apart from Pt–Ir where there was a gradual increase, again due to the decreasing hydrogenolysis activity of this catalyst. In general, catalysts containing germanium, such as Pt–Ir–Ge and Ir–Ge, were found to have slightly higher hydrocracking activities (this is more apparent when data for products such as propane are included). This has been noted in a number of studies [24,38] and has been attributed to the acidity of GeO_2.

The hydrogenolysis selectivities of Pt, Pt–Sn and Pt–Ge were found to have similar values initially. This was perhaps surprising as many studies have found that the addition of tin and germanium to platinum decreases the hydrogenolysis activity [23,24,35]. However, these initial values were obtained after 1 h on line and it is likely that the hydrogenolysis activity of the platinum catalyst had dropped significantly during this time due to coke formation on the metal.

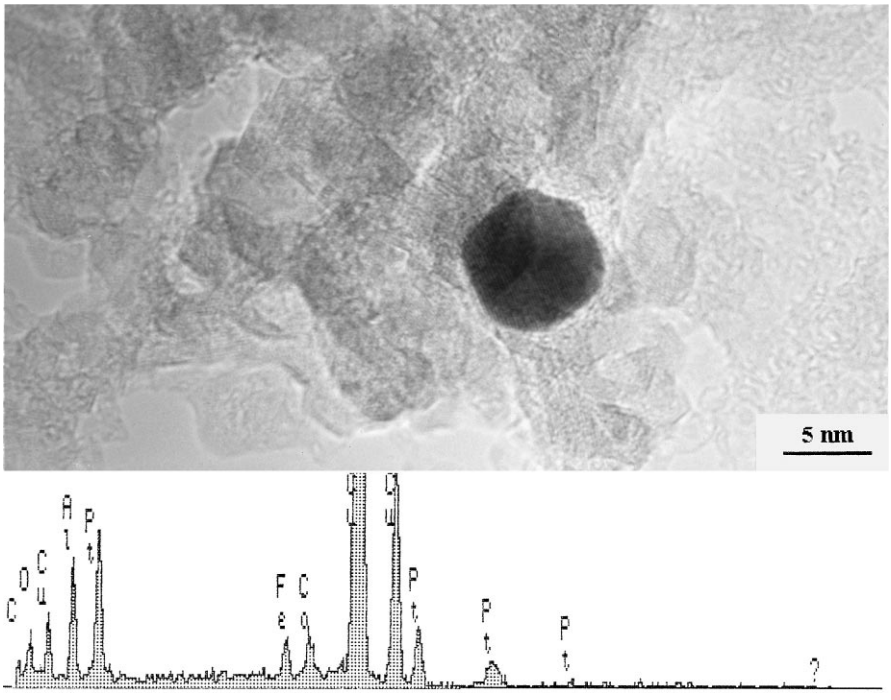

Fig. 7. Pt–Re catalysts after 140 h on line. TEM micrograph and corresponding EDX spectrum. Insert: MBED pattern indexed as [0 1 1] pattern of platinum.

Pt–Re and Pt–Ir, as expected, were found to have higher initial hydrogenolysis activities.

3.2.2. *Pt–Ir–0.03Ge, Pt–Ir–0.3Ge, Ir–Ge and Ir–V*

A graph of conversion versus time for the catalysts Pt–Ir–0.03Ge, Pt–Ir–0.3Ge and Ir–Ge is given in Fig. 12. Pt and Pt–Ir are also included for comparison. The Pt–Ir–0.3Ge catalyst followed a similar deactivation curve to the Pt–Ge catalyst. However, the Pt–Ir–0.03Ge catalyst was observed to be much more resistant to deactivation. The level of conversion over this catalyst remained even above that of Pt-Ir. The Ir–Ge catalyst was also observed to deactivate much more slowly than the related Pt–Ir–0.3Ge and Pt–Ge catalysts.

Although the addition of germanium to catalysts containing iridium modified the conversion levels, a much more pronounced effect was observed on the selectivities, as shown in Table 2. The main effect was a large decrease in the high selectivity of these catalysts towards hydrogenolysis. This produced a corresponding increase in selectivity to the remaining, more desirable, reforming products. However, for Pt–Ir–0.3Ge, as with Pt–Ge, both the selectivity to aromatics and the total conversion fell significantly during the length of the run.

For the Pt–Ir–0.03Ge catalyst the selectivity to aromatics actually increased throughout the run. Although the initial selectivity to hydrogenolysis for this catalysts was very high (35.3%), this value fell very rapidly and after 10 h on line had dropped below

Table 2
Selectivities to the major reforming reactions over Pt–Ir, Pt–Ir–0.3Ge and Pt–Ir–0.03Ge catalysts

Reaction	Selectivity					
	Pt–Ir		Pt–Ir–0.3Ge		Pt–Ir–0.03Ge	
	I	*F*	*I*	*F*	*I*	*F*
Aromatisation	21.7	35.8	37.1	29.6	34.3	45.5
Isomerisation	0.0	0.0	5.5	20.0	0.5	3.1
Hydrocracking	1.4	7.5	20.0	18.8	4.6	14.6
Hydrogenolysis	42.8	22.3	5.6	4.4	35.3	8.5

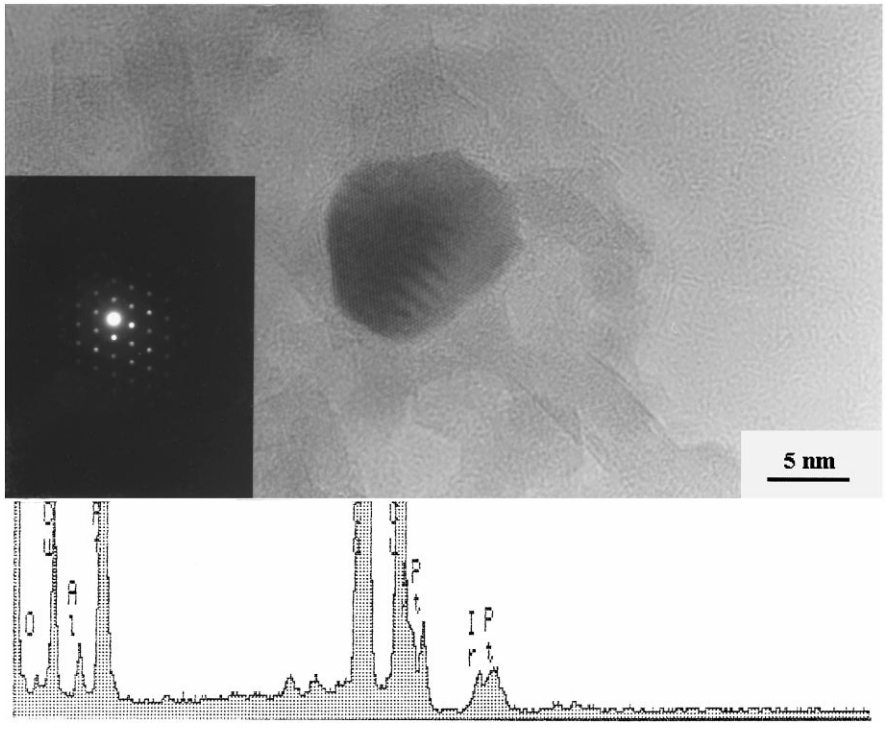

Fig. 8. Pt–Ir–0.03Ge catalysts after 140 h on line. TEM micrograph and corresponding EDX spectrum. Pt/Ir atomic ratio=1.2. Insert: MBED pattern indexed as [0 1 1] pattern of platinum.

10%. The selectivity to this reaction then continued to decrease more gradually. This rapid decrease in hydrogenolysis activity coincided with a rapid increase in the selectivity to aromatisation, which after 6 h on line reached a value of 41.2% and then continued to increase gradually.

The influence of germanium on the structure sensitive hydrogenolysis reaction was even more pronounced on the Ir–Ge catalyst, as shown in Table 3. Pure iridium had an initial selectivity to hydrogenolysis of 100%. With continued use this was slowly poisoned by coke formation on the metal and as a result small amounts of the other reforming products were produced. Addition of germanium to this system very effectively poisoned hydrogenolysis and therefore increased the selectivity to aromatisation, isomerisation and hydrocracking. It is interesting to note that the Ir–Ge catalyst had the highest hydrocracking activity of any of the catalysts studied.

Oxides which exhibit strong metal support interactions have been found to produce similar reductions in hydrogenolysis activity [48,49]. For this reason an Ir–V/Al_2O_3 catalyst was prepared and tested. Although a large decrease in hydrogenolysis activity was observed for Ir–V/Al_2O_3 as compared to Ir/Al_2O_3 under the conditions used in this study, this suppression in hydrogenolysis activity was not as great as on addition of germanium to Ir/Al_2O_3.

Table 3
Selectivities to the major reforming reactions over Ir, Ir–Ge and Ir–V catalysts

Reaction	Selectivity					
	Ir		Ir–Ge		Ir–V	
	I	*F*	*I*	*F*	*I*	*F*
Aromatisation	0.0	6.0	33.6	32.2	27.6	26.9
Isomerisation	0.0	2.2	0.0	10.8	6.9	11.8
Hydrocracking	0.0	2.2	21.0	21.5	14.0	19.0
Hydrogenolysis	100.0	80.7	3.8	2.9	19.1	10.5

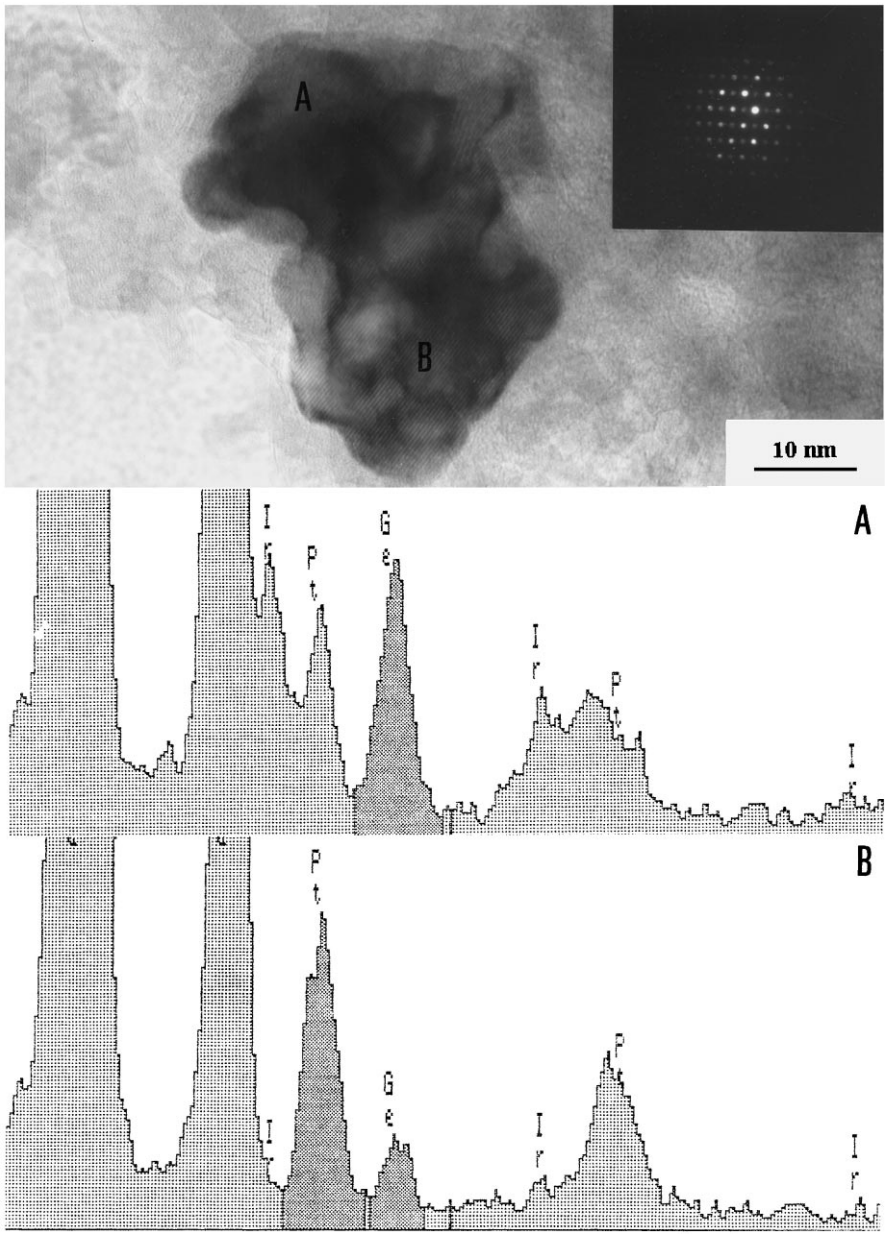

Fig. 9. Pt–Ir–0.3Ge catalysts after 140 h on line. TEM micrograph and corresponding EDX spectra. Region A (a) – Pt/Ir=0.8, Pt+Ir/Ge=1.3. Region B (b) – Pt+Ir/Ge=4.2. Insert: MBED pattern indexed as platinum [0 1 1] pattern (bright spots) with extra superlattice reflections.

3.3. Chemisorption

The chemisorption results are presented in Table 4. Metallic platinum and iridium adsorb both CO and O_2 whilst Ge^0 adsorbs only O_2 [51].

The ability of highly dispersed iridium to show adsorption stoichiometries greater than unity have been reported previously for H_2 [31,40,50] and CO [40,50]. Although a lack of detailed knowledge regarding the stoichiometries of CO and O_2 adsorption

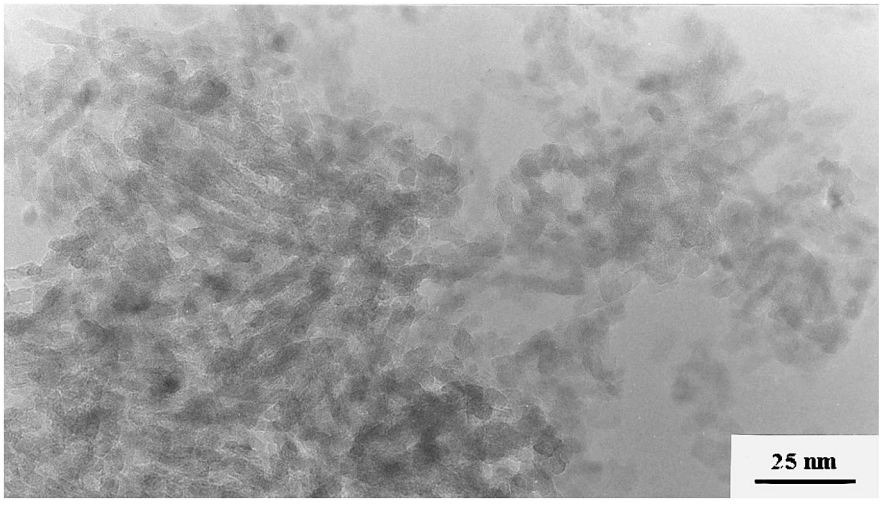

Fig. 10. Ir–Ge catalysts after 140 h on line. TEM micrograph showing typical area of the support.

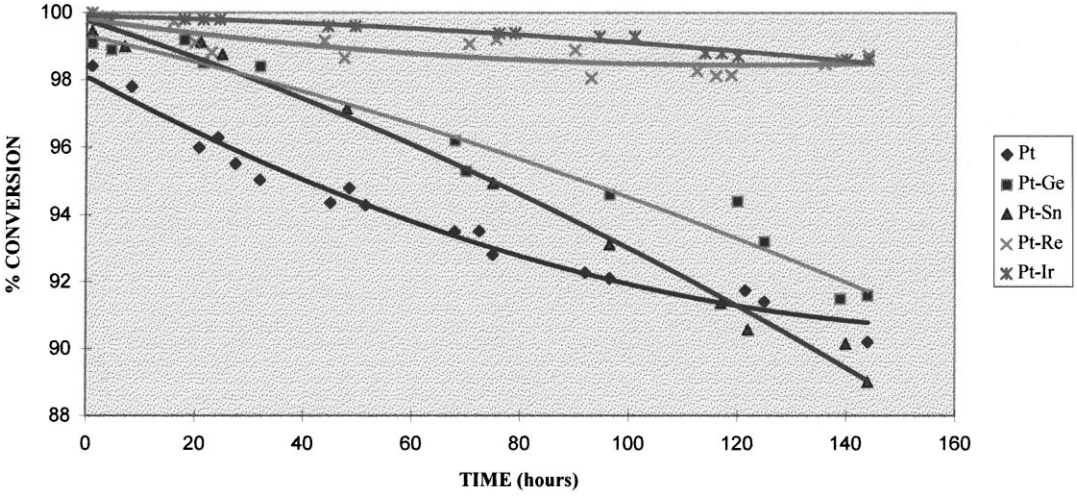

Fig. 11. Graph of conversion versus time on line for catalysts Pt, Pt–Sn, Pt–Ge, Pt–Re and Pt–Ir.

Table 4
Chemisorption results for Ir, Ir–Ge and Pt–Ir–0.3Ge catalysts

Catalyst	Adsorbate	
	CO/M	O/M
Ir	1.18	1.78
Ir–Ge	0.61	1.47
Pt–Ir–0.3Ge	0.43	0.93

on iridium prevented calculation of metal dispersions, some useful quantitative conclusions could still be drawn from these results.

The TEM studies revealed that both Ir and Ir–Ge were highly dispersed with particle sizes $\leq$1 nm. It is therefore unlikely that the difference in CO/M and O/M ratios obtained for these catalysts were due to particle size effects. It is more likely that dilution of the iridium surface by germanium resulted in the observed decrease in adsorption.

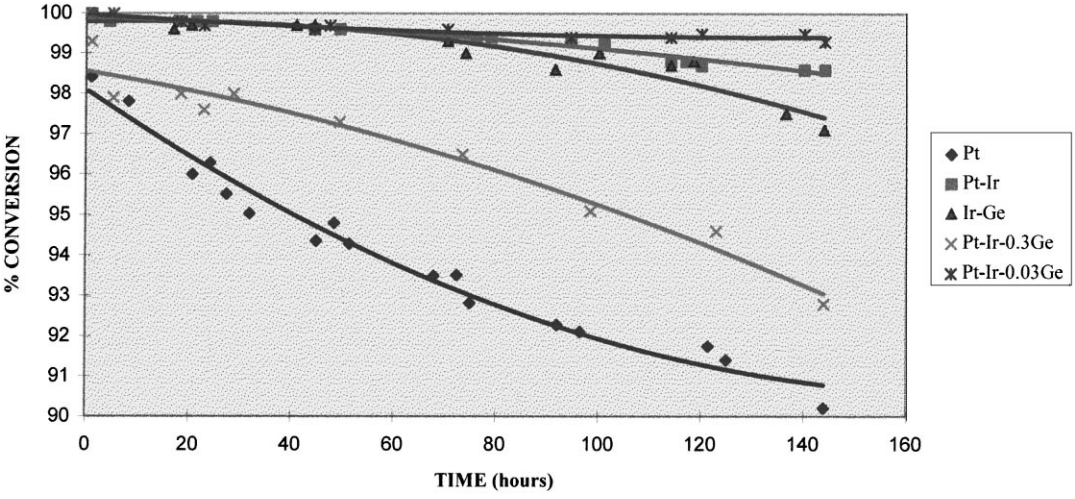

Fig. 12. Graph of conversion versus time on line for catalysts Pt, Pt–Ir, Ir–Ge, Pt–Ir–0.3Ge and Pt–Ir–0.03Ge.

TEM observations of the Pt–Ir–0.3Ge catalyst revealed a slight increase in particle size compared with the two preceding catalysts. It is therefore likely that at least part of the further chemisorption suppression observed on addition of Pt was due to a decrease in dispersion. However, it is also likely that alloy formation between Pt and Ir played a significant role.

3.4. Carbon deposition

Table 5 gives the percentage of carbon by weight deposited on each catalyst after 140 h on line.

These results show that there is no simple relationship between the rate of deactivation and the amount of coke produced. It is known that the type of coke produced and where that coke is deposited are also important factors [41]. In general, Pt–Sn and Pt–Re produced slightly less coke than monometallic platinum. Catalysts containing germanium appeared to produce more coke whilst Ir, Pt–Ir and Ir–V produced very little coke.

Table 5
Weight per cent of carbon deposited on catalysts after 140 h on line

Catalyst	Coke (wt%)
Pt	3.49
Pt–Ge	3.74
Pt–Sn	2.51
Pt–Re	2.22
Pt–Ir	0.93
Pt–Ir-0.03Ge	2.35
Pt–Ir–0.3Ge	3.95
Ir	0.9
Ir–Ge	3.91
Ir–V	0.56

4. Discussion

4.1. Pt–Sn and Pt–Ge

The reforming data clearly show that addition of tin and germanium to Pt/Al_2O_3 improves both the initial activity and selectivity of these catalysts and prevents the initial rapid activity decline that occurs on monometallic platinum.

The strong depression of hydrogenolysis that occurred when germanium was added to an iridium catalyst suggests that a very strong geometric interaction occurred, even though the percentage of germanium present as Ge^0 may have been small. This geometric effect may have been produced by GeO_x species as proposed by Miguel et al. [23,24]. The germanium diluted the active metal surface into smaller groups or ensembles of metal atoms thereby poisoning structure sensitive reactions such as hydrogenolysis and coke formation on the metal. This interaction was also responsible for the reduction in

chemisorption capacity observed on adding Ge to Ir/Al_2O_3. It is likely that a similar interaction occurred between germanium and platinum, and also between tin and platinum, resulting in a decrease in the rate of deactivation due to coking. This occurred even though the overall quantity of coke deposited on these catalysts was not significantly reduced.

However, prolonged use of these catalysts in reforming resulted in the formation of bulk Pt–Ge and Pt–Sn alloys which may have been responsible for the increased rate of deactivation that occurred in these catalysts. A number of studies have found that the presence of relatively large quantities of Sn^0 can poison the activity of these systems [35,52,53]. It has also been found that many of these alloys have a surface which is rich in tin, resulting in loss of active metal surface area [54,55].

4.2. Pt–Re and Pt–Ir

Although TEM could find no evidence for metallic rhenium in the form of Pt–Re alloys, certain similarities in the reforming yields obtained over these two catalysts suggested that at least a fraction of the rhenium present in the Pt–Re catalyst was in the metallic state. Table 6 contains the initial yields of methane over Pt, Pt–Re and Pt–Ir and also the distribution of aromatic products over these catalysts.

Both Pt–Re and Pt–Ir showed a marked increase in hydrogenolysis activity which was attributed to the presence of Re^0 and Ir^0. Also, over platinum the main aromatic products were xylenes and ethylbenzene, while over Pt–Ir the main aromatic products were benzene and toluene. In the case of Pt–Re, there was also a marked shift towards the production of C_6 and C_7 aromatics at the expense of C_8 aromatics, again inferring that some Re^0 was present in this catalyst.

Table 6
Initial yields of methane and distribution of aromatics over Pt, Pt–Re and Pt–Ir

Product	Yield		
	Pt	Pt–Re	Pt–Ir
Methane	5.8	10.0	42.8
C_6+C_7 aromatics	5.0	14.0	21.0
C_8 aromatics	38.4	31.4	0.7

The fact that these trends were much more significant over Pt–Ir than Pt–Re may be because only a small proportion of the Re was reduced to Re^0. However, it must also be remembered that although the hydrogenolysis activity of rhenium is higher than platinum, it is lower than that of iridium [56]. Therefore Pt–Re should not be expected to show the same level of hydrogenolysis activity as Pt–Ir.

There are a number of possible reasons why no Pt–Re alloys were detected by TEM and EDX. One is that the concentration of Re^0 in the particles analysed was below the detection limits of the EDX system. It is also possible that some oxidation of rhenium occurred after removal of the catalyst sample from the reactor and exposure to air prior to transfer to the microscope. Sinfelt and coworkers [57], studying a series of Pd–Re catalysts using EXAFS, found evidence for oxidation of rhenium on switching from a hydrogen to a nitrogen atmosphere. It was concluded by these authors that after changing to nitrogen some Re^0 reacted with lattice oxygen from the Al_2O_3 support.

Both Pt–Re and Pt–Ir catalysts deactivated very slowly. This has been attributed by a number of studies to the ability of metallic rhenium and iridium to prevent coke formation on the metal by hydrogenolysis/hydrogenation of coke fragments or the precursors of coke (e.g. compounds with cyclopentane rings) [39,40]. Indeed, in this study both catalysts produced less coke than Pt/Al_2O_3, although the type of coke produced and where it was deposited are likely to be more important than the overall quantity.

It must be remembered that Pt–Re and Pt–Ir catalysts are both treated with sulphur prior to use in industrial reforming operations. It is not clear whether any of the beneficial hydrogenolysis activity associated with these catalysts would survive this treatment and therefore contribute to the overall stability of these catalysts, or whether under sulphided conditions the improved stability is purely down to ensemble size reduction as proposed by Ribeiro and coworkers [33]. This is particularly true in the case of Pt–Re where sulphur is known to bind preferentially to rhenium.

4.3. Pt–Ir–0.3Ge and Pt–Ir–0.03Ge

The main effect of germanium in these systems was to decrease the hydrogenolysis activity. Again this was

due to a geometric effect. However, in the Pt–Ir–0.3Ge catalysts the formation of bulk Pt–Ir–Ge alloys contributed to the overall rate of deactivation in a similar manner to both Pt–Ge and Pt–Sn. When the concentration of germanium was reduced to 0.03 wt%, initially the hydrogenolysis activity was very high. However, this was very quickly deactivated. One possible explanation for this observation was that initially the small concentration of germanium present was widely dispersed on the surface of the alumina, most likely as an oxide species. Over time the concentration of this germanium in contact with metal particles increased. This could occur either by migration of germanium oxide species over the support surface until contact was made with metal particles, possibly resulting in reduction, or by migration of Ge^0 which had been formed by reaction with hydrogen spilt-over from the metal to the support. As the metal surface was diluted by germanium the selectivity to the structure sensitive hydrogenolysis reaction decreased and the selectivity to the remaining reactions increased. Even after 140 h on line the selectivity to aromatics over these catalysts was still increasing.

The level of conversion over the Pt–Ir–0.03Ge also remained above that of the Pt–Ir catalyst. This suggests that the presence of small quantities of germanium actually increased the resistance to deactivation of these catalysts, even though the total amount of coke produced was significantly increased as compared with the Pt–Ir catalyst.

4.4. Ir, Ir–Ge and Ir–V

The metallic component in these three catalysts was found to show very little evidence of sintering even after 140 h at 510°C in a hydrogen-rich atmosphere. This contrasts with the platinum containing catalysts where a significant proportion of the particles detected had diameters in excess of 20 nm after this time.

Dilution of the surface of iridium by Ge^0 or vanadium oxide species was believed to be responsible for the large suppression in hydrogenolysis activity in these systems. However, it is not clear why the Ir–Ge catalyst produced a relatively large quantity of coke (3.91 wt%) whilst the Ir–V produced a quantity similar to that of Ir (~0.9 wt%).

5. Conclusions

1. Addition of Ge (or Sn) to Pt, Ir or Pt–Ir catalysts dilutes the active metal surface. This geometric effect improves the selectivity of the catalyst and increased its resistance to deactivation.
2. The formation of bulk Pt–Ge, Pt–Sn and Pt–Ir–Ge alloys contributes to the overall rate of deactivation of these systems.
3. Although TEM/EDX studies on the Pt–Re catalyst found no evidence for Re^0 or Pt–Re alloys, the reforming data indicate that a significant proportion of rhenium was present as Re^0.
4. Both Pt–Ir and Pt–Re are highly resistant to deactivation. Metallic Ir and Re provided sites for the hydrogenation/hydrogenolysis of coke fragments and therefore reduced the rate of deactivation of these catalysts.
5. Metallic iridium was found to sinter much less readily in hydrogen at 510°C than metallic platinum.

Acknowledgements

EPSRC are acknowledged for the award of a Ph.D. studentship (NM) at the University of Glasgow.

References

[1] H.E. Klulsdahl, US Patent 3 415 737 (1968).
[2] J.H. Sinfelt, US Patent 3 953 368 (1979).
[3] A.C. Muller, P.A. Engelhard, J.E. Weisang, J. Catal. 56 (1975) 65.
[4] R. Bouwman, P. Biloen, J. Catal. 48 (1979) 209.
[5] M.F.L. Johnson, V.M. Leroy, J. Catal. 35 (1974) 434.
[6] C.L. Pieck, P. Marecot, C.A. Querini, J.M. Parera, J. Barbier, Appl. Catal. 133 (1995) 281.
[7] H.C. Yao, M. Shelef, J. Catal. 44 (1976) 392.
[8] C. Bolivar, R. Charcosset, R. Fréty, M. Primet, L. Tournayan, C. Betizeau, G. Leclercq, R. Maurel, J. Catal. 39 (1975) 249.
[9] B.D. McNicol, J. Catal. 46 (1977) 438.
[10] B.H. Isaacs, E.E. Petersen, J. Catal. 77 (1982) 43.
[11] N. Wagstaff, R.J. Prins, J. Catal. 59 (1979) 434.
[12] R.J. Burch, J. Catal. 71 (1981) 348.
[13] R. Srinivasan, L.A. Rice, B.H. Davis, J. Catal. 129 (1991) 257.
[14] A. Caballero, H. Dexpert, B. Didillon, F. Lepeltier, O. Clause, J. Lynch, J. Phys. Chem. 97 (1993) 11283.
[15] R. Burch, L.C. Garla, J. Catal. 71 (1981) 360.

[16] K. Balakrishnan, J. Schwank, J. Catal. 127 (1991) 287.
[17] M.C. Hobson, S.L. Goresh, G.P. Khare, J. Catal. 142 (1993) 641.
[18] G.T. Baronetti, S.R. de Miguel, O.A. Scelza, A.A. Castro, Appl. Catal. 24 (1986) 109.
[19] E. Merlen, P. Beccat, J.C. Bertolini, P. Delichere, N. Zanier, B. Didillion, J. Catal. 159 (1996) 178.
[20] B.D. McNicol, Paper Presented at the Surface Reactivity and Catalysis Group Meeting, Nottingham, UK, 1976.
[21] J. Goldwasser, A. Bernardo, C. Bolivar, G. Castro, A. Rodriques, A. Fleitas, J. Giron, J. Catal. 100 (1986) 75.
[22] R. Bouwmann, P. Biloen, J. Catal. 48 (1977) 209.
[23] S.R. Miguel, O.A. Scelza, A.C. Castro, Appl. Catal. 44 (1988) 23.
[24] S.R. Miguel, J.A.M. Correa, G.T. Baronetti, A.A. Castro, O.A. Scelza, Appl. Catal. 60 (1990) 47.
[25] J.N. Beltramini, D.L. Trimm, Proceedings of the Ninth International Congress on Catalysis, vol. 3, 1988, p. 1268.
[26] N. Wagstaff, R. Prins, J. Catal. 59 (1979) 446.
[27] K. Foger, H. Jaeger, J. Catal. 67 (1981) 252.
[28] N. Wagstaff, R. Prins, J. Catal. 67 (1981) 255.
[29] Y.-J. Huang, S.C. Fung, W.E. Gates, G.B. McVicker, J. Catal. 118 (1989) 192.
[30] J.H. Sinfelt, G.H. Via, J. Catal. 56 (1979) 1.
[31] R.L. Garten, J.H. Sinfelt, J. Catal. 62 (1980) 127.
[32] J.H. Sinfelt, G.H. Via, F.W. Lytle, J. Chem. Phys. 76 (1982) 2779.
[33] A.L. Bonivardi, F.H. Ribeiro, G.A. Somorjai, J. Catal. 160 (1996) 269.
[34] C. Betizeau, G. Lerercq, R. Maurel, C. Bolivar, H. Charcosset, L. Tournayan, J. Catal. 45 (1976) 179.
[35] B. Coq, F. Figueras, J. Catal. 85 (1984) 197.
[36] F.H. Ribeiro, A.L. Bonivardi, C. Kim, G.A. Somorjai, J. Catal. 150 (1994) 186.
[37] P. Biloen, F.M. Duatzenberg, W.M.H. Sachtler, J. Catal. 50 (1977) 77.
[38] P. Biloen, J.N. Helle, H. Verbeek, F.M. Dautzenberg, W.M.H. Sachtler, J. Catal. 63 (1980) 112.
[39] J.M. Parera, J.N. Beltramini, J. Catal. 112 (1988) 357.
[40] J.L. Carter, G.B. McVicker, W. Weissman, W.S. Kmak, J.H. Sinfelt, Appl. Catal. 3 (1982) 327.
[41] J. Beltramini, D.L. Trimm, Appl. Catal. 32 (1987) 71.
[42] Z. Huang, J.R. Fryer, C. Park, D. Stirling, G. Webb, J. Catal. 148 (1994) 478.
[43] Z. Huang, J.R. Fryer, C. Park, D. Stirling, G. Webb, J. Catal. 159 (1996) 340.
[44] Z. Huang, J.R. Fryer, D. Stirling, G. Webb, Phil. Mag. A 72 (1995) 1495.
[45] Z. Huang, J.R. Fryer, C. Park, D. Stirling, G. Webb, J. Catal. 175 (1988) 226.
[46] C. Park, G. Webb, in preparation.
[47] S.D. Jackson, B.M. Glanville, J. Willis, G.D. McLellan, G. Webb, R.B. Moyes, S. Simpson, P.B. Wells, R. Whyman, J. Catal. 137 (1993) 207.
[48] A.J. Den Hartog, A.G.T.M. Bastein, V. Ponec, J. Mol. Catal. 52 (1993) 129.
[49] G. Bond, S. Flamerz, J. Chem. Soc., Faraday Trans. 87(5) (1991) 767.
[50] G.B. McVicker, P.J. Collins, J.J. Ziemak, J. Catal. 74 (1982) 156.
[51] G.C. Bond, Catalysis by Metals, Academic Press, London, 1962.
[52] Y. Fan, Z. Xu, J. Zang, L. Lin, in: C.H. Bartholomew, J.B. Butt (Eds.), Catalyst Deactivation, Elsevier, Amsterdam, 1991, p. 683.
[53] Y. Fan, L. Lin, J. Zang, Z. Xu, in: Proceedings of the 10th International Congress on Catalysis, Elsevier, Amsterdam, 1992, p. 2507.
[54] R.A. van Santen, W.M.H. Sachtler, J. Catal. 33 (1974) 202.
[55] R. Bouwman, P. Biloen, Surf. Sci. 41 (1974) 348.
[56] J.H. Sinfelt, Adv. Catal. 23 (1973) 91.
[57] G. Meitzner, G.H. Via, F.W. Lytle, J.H. Sinfelt, J. Chem. Phys. 87 (1987) 6354.